Appl. Sci. Converg. Technol. 28(6): 217-220 (2019)
https://doi.org/10.5757/ASCT.2019.28.6.217
eISSN : 2288-6559

Research Paper

Effect of Deposition Sequence in MoO_3 and HAT-CN Dual-anode Buffer Layer on Inverted Organic Photovoltaics

Received November 15, 2019; accepted November 22, 2019

Seungsun Choi, Wonsik Kim, Woojin Shin, Sohyun Park, and Hyunbok Lee*

Department of Physics, Kangwon National University, Gangwon-do 24341, Republic of Korea

***Corresponding author E-mail:** hyunbok@kangwon.ac.kr

ABSTRACT

Interface engineering plays a critical role in the device performance of organic photovoltaics (OPVs). In inverted OPVs, the top anode must have a high work function to match the highest occupied molecular orbital level of a p-type organic semiconductor. Therefore, a functional interlayer with a high work function is inserted between the light-absorbing layer and anode. OPVs with a dual-anode buffer layer have been reported to exhibit a superior performance than those with a single-anode buffer layer. Herein, the device performance of inverted OPVs with a poly(3-hexylthiophene-2,5-diyl):[6,6]-phenyl-C_{61}-butyric acid methyl ester light-absorbing layer and dual-anode buffer layer of MoO_3 and 1,4,5,8,9,11-hexaazatriphenylenehexacarbonitrile (HAT-CN) is investigated. The power conversion efficiency (PCE) of the OPV with the HAT-CN/MoO_3/Al anode system is lower than that with the conventional MoO_3/Al anode system. However, the PCE of the OPV with MoO_3/HAT-CN/Al is slightly higher than that with MoO_3/Al. The change in the device performance by varying the deposition sequence of HAT-CN and MoO_3 is discussed based on the built-in potential.

Keywords: Inverted organic photovoltaics, Anode buffer layer, MoO_3, HAT-CN, Interface engineering

I. Introduction

Organic photovoltaics (OPVs) have attracted significant attention owing to their low-cost fabrication, low weight, and mechanical flexibility [1-3]. Generally, OPVs have a sandwich structure with an organic light-absorbing layer between the anode and cathode. In this multilayer structure, interface engineering between the organic semiconductor and metal electrodes plays an important role in the device performance [4-6]. To attain high device performance, the basic requirement of the anode is a high work function. To increase the work function, a functional interlayer is inserted between the anode and p-type organic semiconductor. Additionally, an inverted structure of the OPVs, where the top electrode is used as an anode, is known to have a long device lifetime [7]. However, Al and Ag, which are commonly used as the top electrode materials, have low work functions that do not match the highest occupied molecular orbital (HOMO) level of a conventional p-type organic semiconductor. Therefore, a suitable anode buffer layer, such as MoO_3, should be used to form an efficient energy-level alignment [8]. In addition, MoO_3 enables charge generation owing to the deep conduction band minimum [9]. Hence, MoO_3 is frequently inserted between the organic light-absorbing layer and top anode in inverted OPVs. However, it has been recently reported that MoO_3 cannot achieve a perfect Ohmic contact, and therefore, an additional organic layer should be inserted between MoO_3 and p-type organic semiconductors for further enhancement of the hole transport [10]. Some functional materials have been incorporated into MoO_3, and the dual-anode buffer layer has shown a more enhanced device performance. For example, OPVs with a MoO_3 and CuI dual-anode buffer layer exhibit a better power conversion efficiency (PCE) than a single MoO_3 or CuI buffer layer [11]. As a similar strategy, in an inverted top-emission organic light-emitting diode, a 1,4,5,8,9,11-hexaazatriphenylenehexacarbonitrile (HAT-CN) and MoO_3 dual-anode buffer layer has been reported to exhibit superior performance than a single MoO_3 anode buffer layer [12]. However, this HAT-CN and MoO_3 dual-anode buffer layer has not been employed in inverted OPVs.

In this study, a dual-anode buffer layer consisting of MoO_3 and HAT-CN is investigated in inverted OPVs. The MoO_3 and HAT-CN layers are deposited onto the poly(3-hexylthiophene-2,5-diyl) (P3HT):[6,6]-phenyl-C_{61}-butyric acid methyl ester (PCBM) bulk hetero-junction layer by varying the deposition sequence. Thereafter, the device performances of the OPVs and hole-only devices with the MoO_3/Al, HAT-CN/MoO_3/Al, and MoO_3/HAT-CN/Al anode systems are compared. The possible cause of the differences in the device performance is discussed based on the capacitance-voltage measurements.

II. Experimental details

The inverted OPVs were fabricated with an Al/anode buffer layer/P3HT:PCBM/polyethylenimine ethoxylated (PEIE)/indium tin oxide (ITO) structure. An ITO-patterned glass substrate was cleaned by ultrasonication in deionized water, detergent, acetone, and methanol

bath. It was then dried with N_2 gas flow and treated with ultraviolet ozone at 100 °C for 15 min. At the cathode buffer layer, PEIE (Sigma-Aldrich) was deposited by spin coating onto ITO at a spin rate of 5000 rpm for 60 s [13]. Subsequently, the sample was annealed at 100 °C for 10 min. P3HT (Mw: > 45,000, regioregularity: > 93 %) and PCBM (purity: > 99.5 %) were purchased from Luminescence Technology. P3HT and PCBM were dissolved in chlorobenzene (purity: > 99.9 %, Sigma-Aldrich) at a concentration of 80 mg mL^{-1} (1:1 wt %) and stirred overnight before use. The P3HT:PCBM light-absorbing layer was deposited by spin coating onto PEIE/ITO from the mixed solution at a spin rate of 2000 rpm for 60 s. Then, the film was annealed at 150 °C for 15 min. All solution processes were accomplished at ambient conditions, and the annealing was performed using a hot plate. The sample was thereafter transferred into a vacuum chamber. MoO_3 (purity: > 99.97 %) was purchased from Sigma-Aldrich and HAT-CN (purity: > 99.9 %) from EM INDEX. MoO_3 (15 nm) and HAT-CN (5 nm) were deposited via thermal evaporation at a deposition rate of 0.01 nm s^{-1}. Finally, the 100 nm-thick Al layer was deposited via thermal evaporation with deposition rates of 0.01 nm s^{-1} for the initial 10 nm thickness and 0.05 – 0.1 nm s^{-1} for a thickness of 90 nm. The hole-only devices were fabricated with the Al/anode buffer layer/P3HT/poly(3,4-ethylenedioxythiophene)-poly(styrene sulfonate) (PEDOT:PSS)/ITO structure. PEDOT:PSS (Clevios™ P VP AI 4083) was purchased from Heraeus. The PEDOT:PSS layer was deposited onto ITO by spin coating at a rate of 500 rpm for the initial 5 s, followed by 3000 rpm for the next 30 s, and then annealed at 150 °C for 10 min. Subsequently, the P3HT layer was deposited onto PEDOT:PSS/ITO by spin coating from a chlorobenzene solution at a concentration of 40 mg mL^{-1}, and then annealed at 150 °C for 15 min. The anode buffer layer and Al were deposited in the same manner as the OPVs. The device area of the OPVs and hole-only devices was 0.04 cm^2.

Current density-voltage (*J-V*) characteristics were measured using a Keithley 2400 source measure unit. The photovoltaic parameters were recorded under Air Mass 1.5G 1 sun illumination generated by a solar simulator (Model 10500, Abet Technologies). Capacitance-voltage (*C-V*) measurements were performed using a Solartron SI 1260 impedance/gain-phase analyzer. All measurements were performed at room temperature and ambient conditions. For the *C-V* measurements, a frequency of ~1000 kHz, in which the phase of impedance showed the closest value to 90°, was used. AC perturbation of 25 mV was employed.

III. Results and discussion

Figure 1 shows (a) the chemical structures of the organic materials (P3HT, PCBM, and HAT-CN), and (b) the energy-level alignment of the OPVs with the MoO_3 and HAT-CN dual-anode buffer layer used in this study. The energy levels are obtained from the charge transport levels measured by ultraviolet and inverse photoelectron spectroscopy [9,14,15] under the assumption of vacuum-level alignment. P3HT and PCBM were used as the donor and acceptor, respectively. Owing to the low work function of PEIE, the cathode interface was efficiently contacted. HAT-CN has a deep HOMO level and high work function, similar to MoO_3 [15,16]. However, the reported transport gap of HAT-CN is much larger than that of MoO_3.

Figure 2(a) shows the *J-V* characteristics of the inverted OPVs upon 1 sun illumination. The *J-V* curve indicates an average performance among the 32 devices. The inset shows the schematic of the

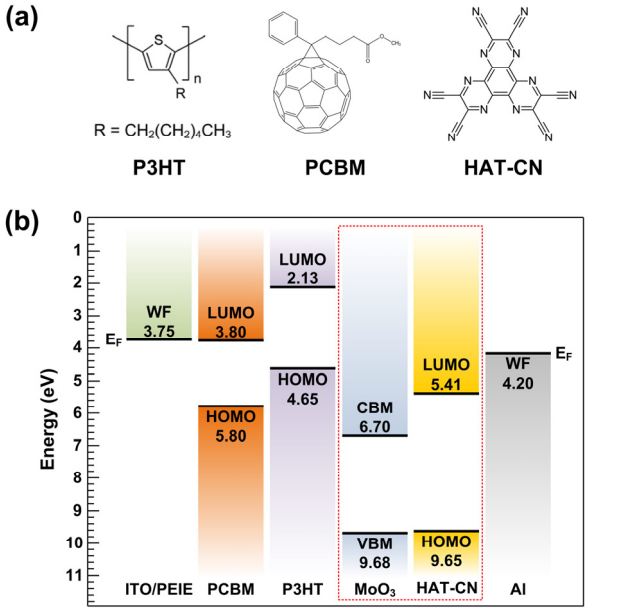

Figure 1. (Color online) (a) Chemical structures of the organic semiconductors used in this study. (b) Energy-level alignment of the inverted OPVs with MoO_3 and HAT-CN dual-anode buffer layer. E_F and WF denote the Fermi level and work function, respectively.

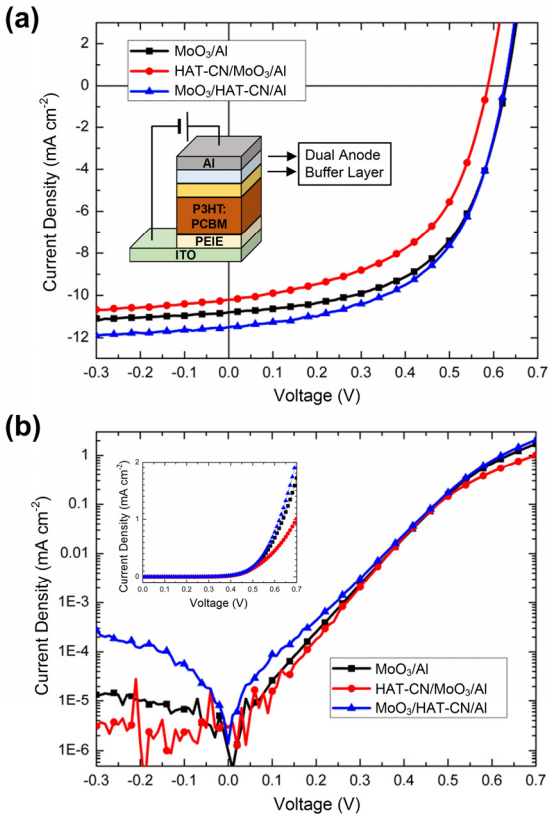

Figure 2. (Color online) (a) *J-V* characteristics of the inverted OPVs with MoO_3/Al (black square), HAT-CN/MoO_3/Al (red circle), and MoO_3/HAT-CN/Al (blue triangle) anode systems upon 1 sun illumination. Inset shows the device structure. (b) Semi-log plot of *J-V* characteristics of the inverted OPVs with MoO_3/Al (black square), HAT-CN/MoO_3/Al (red circle), and MoO_3/HAT-CN/Al (blue triangle) anode systems under dark conditions. Inset shows a linear plot of *J-V* characteristics.

Table I. Photovoltaic parameters of the inverted OPVs using different anode systems. Statistical analysis was performed for 32 devices.

Anode system	J_{SC} (mA cm^{-2})	V_{OC} (V)	FF (%)	PCE (%)
MoO_3/Al	10.60 ± 0.34	0.63 ± 0.004	56.6 ± 2.12	3.74 ± 0.20
HAT-CN/MoO_3/Al	10.28 ± 0.34	0.58 ± 0.008	53.1 ± 1.38	3.19 ± 0.12
MoO_3/HAT-CN/Al	11.40 ± 0.32	0.63 ± 0.005	55.6 ± 1.38	3.97 ± 0.12

inverted OPV device structure. The photovoltaic parameters and OPV statistics are summarized in Table I. The OPVs with a single MoO_3 anode buffer layer show a short-circuit current density (J_{SC}) of 10.60 ± 0.34 mA cm^{-2}, open-circuit voltage (V_{OC}) of 0.63 ± 0.004 V, and fill factor (FF) of 56.6 ± 2.12 %, which yields a PCE of 3.74 ± 0.20 %. However, when the HAT-CN/MoO_3/Al anode system is used, all photovoltaic parameters are significantly reduced. The OPVs with HAT-CN/MoO_3/Al show a J_{SC} of 10.28 ± 0.34 mA cm^{-2}, V_{OC} of 0.58 ± 0.008 V, FF of 53.1 ± 1.38 %, and PCE of 3.19 ± 0.12 %. However, when the MoO_3/HAT-CN/Al anode system is employed, the PCE of the OPVs is only slightly increased. The OPVs with MoO_3/HAT-CN/Al show a J_{SC} of 11.40 ± 0.32 mA cm^{-2}, V_{OC} of 0.63 ± 0.005 V, and FF of 55.6 ± 1.38 %, resulting in a PCE of 3.97 ± 0.12 %. Although the FF of the OPVs with MoO_3/HAT-CN/Al decreases in comparison to that with a single MoO_3 anode buffer layer, V_{OC} does not change, and J_{SC} increases. The reduced FF with the insertion of the additional HAT-CN layer can be attributed to an increase in the series resistance due to an increase in the total thickness. In contrast, the slightly improved J_{SC} values of the OPVs with MoO_3/HAT-CN/Al may be due to the enhancement of the light-absorbing ability via optical interference by the increased thickness [17].

Figure 2(b) shows a semi-log plot of the *J-V* characteristics of the OPVs under dark conditions. The inset shows a linear plot of the *J-V* characteristics. At 0.7 V, the OPV with MoO_3/HAT-CN/Al records the highest *J* value, but similar to that for MoO_3/Al. The OPV with HAT-CN/MoO_3/Al shows the lowest *J* value. The measured *J* values of the OPVs with MoO_3/Al, HAT-CN/MoO_3/Al, and MoO_3/HAT-CN/Al at 0.7 V are 1.72, 1.01, and 2.06 mA cm^{-2}, respectively. Such changes in the device performance by the variation in the deposition sequence of the dual-anode buffer layer have also been observed in previous literature reports [11,12]. These results clearly indicate that the HAT-CN/MoO_3/Al anode system differs from the MoO_3/Al and MoO_3/HAT-CN/Al anode systems.

Figure 3 shows the C^{-2}-*V* and *C-V* characteristics of the inverted OPVs with MoO_3/Al, HAT-CN/MoO_3/Al, and MoO_3/HAT-CN/Al anode systems. The *C-V* characteristics are similar to the *J-V* characteristics shown in Fig. 2. At 0.7 V, the OPV with HAT-CN/MoO_3/Al records the lowest *C* value, while the OPVs with MoO_3/Al and MoO_3/HAT-CN/Al show similar *C* values. These low *J* and *C* values for the OPV with HAT-CN/MoO_3/Al can be attributed to the low built-in potential (V_{bi}). From the Mott-Schottky plot, the V_{bi} value is evaluated using the following equation:

$$C^{-2} = \frac{2}{qA^2\varepsilon N_D}(V_{bi} - V) \quad (1)$$

where *q* is the elementary charge, *A* is the area, ε is the permittivity, and N_D is the doping concentration [18]. Thus, the *x*-intercept of the Mott-Schottky plot provides the V_{bi} value across the device. Through a linear fitting, an identical V_{bi} value of 0.31 V is obtained for the

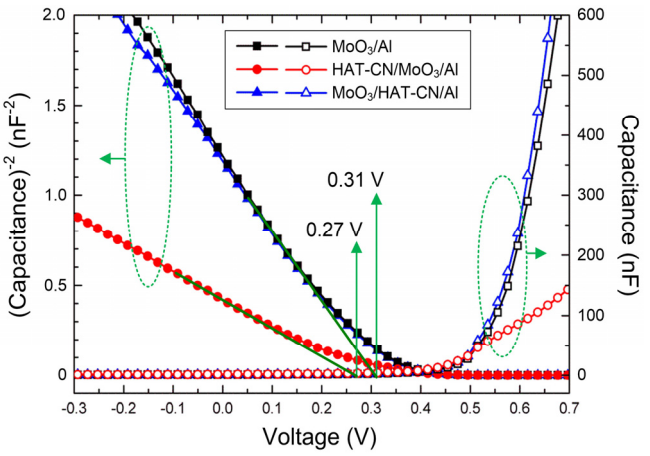

Figure 3. (Color online) C^{-2}-*V* (left axis, filled symbol) and *C-V* (right axis, hollow symbol) characteristics of the inverted OPVs with MoO_3/Al (black square), HAT-CN/MoO_3/Al (red circle), and MoO_3/HAT-CN/Al (blue triangle) anode systems under dark conditions.

OPVs with MoO_3/Al and MoO_3/HAT-CN/Al. However, the OPV with HAT-CN/MoO_3/Al shows a V_{bi} of 0.27 V. This V_{bi} difference matches well with the V_{OC} difference in the OPVs. The V_{OC} values of the OPVs with MoO_3/Al and MoO_3/HAT-CN/Al are identical, but that of the OPV with HAT-CN/MoO_3/Al is lower by 0.05 V. Thus, the low PCE of the OPV with HAT-CN/MoO_3/Al can be mainly attributed to the low V_{bi} formation [19,20]. In addition, the low V_{bi} can increase the interface recombination, which lowers the J_{SC} value. The low V_{bi} indicates a high hole-injection barrier at the anode interface, which results in a low *J* value in the OPVs under dark conditions [Fig. 2(b)]. In contrast, although the V_{bi} value is identical in both the OPVs with MoO_3/Al and MoO_3/HAT-CN/Al, the OPV with MoO_3/HAT-CN/Al shows a high *J* value at 0.7 V under dark conditions compared to that with MoO_3/Al. One possible explanation is the formation of a charge-transfer complex between HAT-CN and Al. When Al is deposited on HAT-CN, a strong chemical reaction occurs between them, and its HOMO level exists close to the Fermi level [16]. This state can assist the hole transport from MoO_3 to Al, thereby increasing the *J* value.

Figure 4 shows the *J-V* characteristics of hole-only devices with the MoO_3/Al, HAT-CN/MoO_3/Al, and MoO_3/HAT-CN/Al anode systems. Through the anode buffer layer, the hole transport direction is from Al to P3HT. Similar to the *J-V* characteristics of the OPVs under dark conditions, the device with MoO_3/HAT-CN/Al shows the highest *J* value at 5 V, and that with HAT-CN/MoO_3/Al shows the lowest *J* value among the devices. The measured *J* values of the hole-only devices with MoO_3/Al, HAT-CN/MoO_3/Al, and MoO_3/HAT-CN/Al at 5 V are 169.1, 131.6, and 185.0 mA cm^{-2}, respectively. This also indicates the low V_{bi} formation by the HAT-CN/MoO_3/Al anode

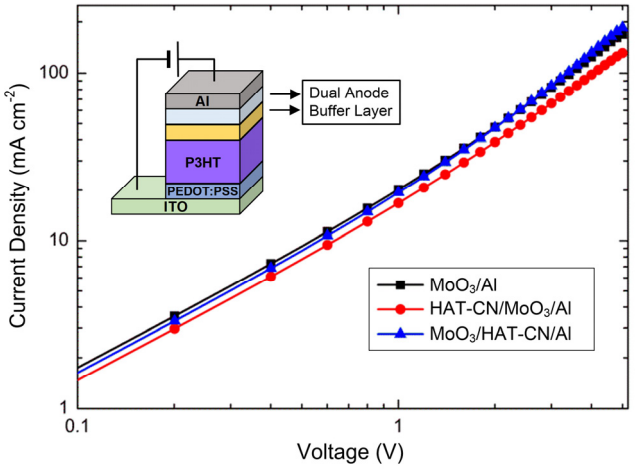

Figure 4. (Color online) *J-V* characteristics of the hole-only devices with MoO_3/Al (black square), HAT-CN/MoO_3/Al (red circle), and MoO_3/HAT-CN/Al (blue triangle) anode systems. Inset shows the device structure.

system. Thus, the deposition sequence in the dual-anode buffer layer can significantly affect the device performance.

IV. Conclusion

In this study, the effect of deposition sequence in a MoO_3 and HAT-CN dual-anode buffer layer on inverted OPVs is investigated. When HAT-CN is deposited prior to MoO_3, the device performance of the OPV significantly deteriorates compared to that with a single MoO_3 anode buffer layer. From the Mott-Schottky plots, it is concluded that the low PCE of the OPVs with HAT-CN/MoO_3/Al is attributed to the low V_{bi}. However, when MoO_3 is deposited prior to HAT-CN, the OPVs show a slightly higher PCE than that with a single MoO_3 anode buffer layer. Thus, although MoO_3 and HAT-CN have similar electronic structures, the deposition sequence in the dual-anode buffer layer significantly influences the device performance of the inverted OPVs.

Acknowledgements

This study was supported by the National Research Foundation of Korea (NRF-2018R1D1A1B07051050 and 2018R1A6A1A03025582) and Supporting Business for College Innovation from Kangwon National University.

References

[1] G. Li, R. Zhu, and Y. Yang, Nat. Photonics 6, 153 (2012).
[2] L. Lu, T. Zheng, Q. Wu, A. M. Schneider, D. Zhao, and L. Yu, Chem. Rev. 115, 12666 (2015).
[3] G. Dennler, M. C. Scharber, and C. J. Brabec, Adv. Mater. 21, 1323 (2009).
[4] N. Koch, ChemPhysChem 8, 1438 (2007).
[5] H. Lee, S. W. Cho, and Y. Yi, Curr. Appl. Phys. 16, 1533 (2016).
[6] R. Steim, F. R. Kogler, and C. J. Brabec, J. Mater. Chem. 20, 2499 (2010).
[7] K. Wang, C. Liu, T. Meng, C. Yi, and X. Gong, Chem. Soc. Rev. 45, 2937 (2016).
[8] H. Lee, S. W. Cho, K. Han, P. E. Jeon, C. N. Whang, K. Jeong, K. Cho, and Y. Yi, Appl. Phys. Lett. 93, 043308 (2008).
[9] M. Kröger, S. Hamwi, J. Meyer, T. Riedl, W. Kowalsky, and A. Kahn, Appl. Phys. Lett. 95, 123301 (2009).
[10] N. B. Kotadiya, H. Lu, A. Mondal, Y. Ie, D. Andrienko, P. W. M. Blom, and G. J. A. H. Wetzelaer, Nat. Mater. 17, 329 (2018).
[11] S. Yoon, H. Kim, E. Y. Shin, I. G. Bae, B. Park, Y. Y. Noh, and I. Hwang, Org. Electron. 32, 200 (2016).
[12] C. H. Park, H. J. Lee, J. H. Hwang, K. N. Kim, Y. S. Shim, S. G. Jung, C. H. Park, Y. W. Park, and B. K. Ju, ACS Appl. Mater. Interfaces 7, 6047 (2015).
[13] Y. Zhou, C. Fuentes-Hernandez, J. Shim, J. Meyer, A. J. Giordano, H. Li, P. Winget, T. Papadopoulos, H. Cheun, J. Kim, M. Fenoll, A. Dindar, W. Haske, E. Najafabadi, T. M. Khan, H. Sojoudi, S. Barlow, S. Graham, J. L. Brédas, S. R. Marder, A. Kahn, and B. Kippelen, Science 336, 327 (2012).
[14] Z. L. Guan, J. B. Kim, H. Wang, C. Jaye, D. A. Fischer, Y. L. Loo, and A. Kahn, Org. Electron. 11, 1779 (2010).
[15] H. Lee, J. Lee, S. Park, Y. Yi, S. W. Cho, J. W. Kim, and S. J. Kang, Carbon 71, 268 (2014).
[16] S. M. Park, Y. H. Kim, Y. Yi, H. Y. Oh, and J. W. Kim, Appl. Phys. Lett. 97, 063308 (2010).
[17] J. Y. Kim, S. H. Kim, H. H. Lee, K. Lee, W. Ma, X. Gong, and A. J. Heeger, Adv. Mater. 18, 572 (2006).
[18] G. Garcia-Belmonte, A. Munar, E. M. Barea, J. Bisquert, I. Ugarte, and R. Pacios, Org. Electron. 9, 847 (2008).
[19] H. Zhou, Y. Zhang, J. Seifter, S. D. Collins, C. Luo, G. C. Bazan, T. Q. Nguyen, and A. J. Heeger, Adv. Mater. 25, 1646 (2013).
[20] C. Zhang, L. Qi, Q. Chen, L. Lv, Y. Ning, Y. Hu, Y. Hou, and F. Teng, J. Mater. Chem. C 2, 8715 (2014).